

RESEARCH ARTICLE

3D-printed artificial cornea featuring aligned fibrous structure and enhanced mechanical strength

Priyanka Chaudhary¹, Dun-Heng Tan^{1,2}, Chia-Hsien Lee¹, Chun-Yu Chang³, Ting-Han Lin⁴, Ming-Chung Wu^{4,5}, Wei-Fang Su^{1,2}, Meng-Fang Lin^{1*}, and Yu-Ching Huang^{1,4,5*}

¹Department of Materials Engineering and Biochemical Technology R&D Center, Ming Chi University of Technology, New Taipei City 24301, Taiwan

²Department of Materials Science and Engineering, National Taiwan University, Taipei City 10617, Taiwan

³Bachelor Program in Semiconductor Materials and Fabrication, Ming Chi University of Technology, New Taipei City 24301, Taiwan

⁴Center for Sustainability and Energy Technologies, Chang Gung University, Taoyuan 33302, Taiwan

⁵Department of Chemical and Materials Engineering, Chang Gung University, Taoyuan 33302, Taiwan

(This article belongs to the *Special Issue: Made-to-order Organ*)

Abstract

The global shortage of donor eye bank tissue has significantly impeded advancements in biomaterial for corneal implantation. To address this issue, we have developed a three-dimensional (3D)-printed artificial cornea using a composite scaffolds of sodium alginate (SA) and cellulose nanofibers (CNF), crosslinked with poly-L-lysine-co-L-glutamic acid (PLL₃₀GA₂₀, PG) and calcium chloride (CaCl₂, CC). The 2 wt% SA/CNF composite scaffolds offer several advantages, including low toxicity, cost-effectiveness, excellent printability, and high mechanical strength, even with low crosslinker concentrations. The PG was synthesized via ring-opening polymerization of L-glutamate N-carboxyl anhydride (BGNCA) and L-lysine N-carboxyl anhydride (CBZNCA). The purity of the monomers was verified through differential scanning calorimetry analysis, revealing a melting point of 97°C. The molecular weight of the synthesized PG was determined to be 47 kDa. A dual crosslinking strategy was employed, starting with electrostatic crosslinking, followed by ionic crosslinking using varying concentrations of PG and CC at different effective charge concentrations of 6.25, 12.25, and 25 mM. The hydrogel and 3D-printed cornea were comprehensively evaluated for chemical structure, surface functional groups, water content, mechanical strength, orientation, cytotoxicity, biocompatibility, and transparency. Notably, the inclusion of PG significantly enhanced the mechanical properties of the 3D-printed cornea, with the hydrogel achieving a storage modulus of 2,360 kPa at 6.25 mM of PG/CC, while maintaining over 95% water content. The artificial cornea demonstrated 86% transparency, and the cell viability showed 96% viable on day 7 with degradation rate of 35.9% in 28 days. The superior hydrophilicity, transparency, and mechanical strength of the printed scaffolds highlights their potential for the development of full-thickness corneal structures, making them a promising candidate for future corneal implants.

*Corresponding authors:

Meng-Fang Lin
(mflin@mail.mcut.edu.tw)

Yu-Ching Huang
(huangyc@mail.mcut.edu.tw)

Citation: Chaudhary P, Tan D-H, Lee C-H, et al. 3D-printed artificial cornea featuring aligned fibrous structure and enhanced mechanical strength.

Int J Bioprint. 2025;11(1):598-613.
doi: 10.36922/ijb.4687

Received: August 29, 2024

Revised: October 15, 2024

Accepted: October 28, 2024

Published Online: October 28, 2024

Copyright: © 2024 Author(s).

This is an Open Access article distributed under the terms of the Creative Commons Attribution License, permitting distribution, and reproduction in any medium, provided the original work is properly cited.

Publisher's Note: AccScience Publishing remains neutral with regard to jurisdictional claims in published maps and institutional affiliations.

Keywords: Scaffold; Poly-L-lysine-co-L-glutamic acid; 3D bioprinting; Artificial cornea

1. Introduction

The cornea is a transparent and well-structured tissue that plays a crucial role in the majority of the eye's refractive power.¹ Damage to the cornea, whether from bacterial infections or injuries, can lead to cell failure, visual impairment, and even blindness.^{2,3} Globally, over 10 million people are affected by various corneal issues each year.⁴ Due to its high short-term success rate, penetrating keratoplasty is the most utilized grafting method to restore vision in cases of severe corneal disorders.⁵ However, the availability of donor corneal tissue is insufficient to meet global demand. Alternative treatments, such as artificial keratoprotheses, decellularized animal corneal tissue (e.g., pig cornea), and human amniotic membrane, have been explored, but these methods often suffer from low success rates or are not universally approved for tissue transplantation.^{6,7}

Biodegradable and biocompatible polymers have emerged as critical components in biomedical engineering, especially in three-dimensional (3D) printing applications such as tissue regeneration scaffolds and drug delivery systems. These biomaterials are of significant attention in cartilage and tissue engineering because they can replicate the properties of the native extracellular matrix, promoting cell adhesion, proliferation, and differentiation. Among the wide variety of polymers used in 3D printing, notable examples include gelatin/gelatin methacryloyl (GelMA), zein, bovine serum albumin, ultra-high molecular weight polyethylene, and polylactic acid. However, each of these materials presents specific limitations concerning mechanical properties, biodegradation rates, and biocompatibility.^{8,9} Additional polymers such as poly(methyl methacrylate) cover both natural and synthetic origins, including collagen, gelatin, chitosan, silk, polyethylene glycol, polycaprolactone, poly(lactic-co-glycolic acid) (PLGA), and poly(2-hydroxyethyl methacrylate). These materials can be used individually or in combination to optimize performance. Polyethylene glycol diacrylate (PEGDA) and GelMA, for example, are photocurable gels that can be crosslinked using visible light irradiation with Lithium phenyl-2,4,6-trimethylbenzoylphosphinate (LAP).¹⁰⁻¹³ In a study by Patel et al.¹⁴, a GelMA-LAP bio-ink system was developed to fabricate 3D-printed osteogenic models using a volumetric approach, where 2D light patterns were synchronously irradiated while rotating.¹⁵ However, these synthetic materials often fail due to poor host-implant integration, leading to inflammation and implant extrusion.¹⁶ Clinical

reports indicate that less than half of patients retain their original keratoprosthesis after follow-up. Biological and biosynthetic materials, such as silk or crosslinked collagen, have shown promise due to their excellent optical transparency and biocompatibility. Despite this, their mechanical integrity is often compromised, requiring overlay sutures instead of standard interrupted sutures. These materials also lack the fibril arrangement of collagen lamellae found in the corneal stroma, which offers low mechanical strength.^{16,17} Another way to enhance the mechanical strength of the hydrogel is dual crosslinking, which combines two forms of crosslinks to create a tough and flexible material. For example, one type of crosslink can provide elasticity while the other adds strength.

Researchers are also working to recreate the complicated lamellar structure of the cornea using biomaterials.¹⁸ Layer-by-layer structural implants have been created using corneal fibroblasts and various substrates, such as gelatin,¹⁹ collagen film,²⁰ silk fibrins, CNF,²¹ and peptide amphiphile.²² Corneal fibroblasts secrete stromal extracellular matrix within the biomaterial scaffold, creating a corneal stromal equivalent.²³ CNF, a nontoxic fibrous material, has shown promise in tissue engineering due to its alignment and high mechanical strength. Previous studies on CNF-containing hydrogels have reported various mechanical properties. For example, Dong et al.²⁴ reported that a 61.25 wt% 2,2,6,6-tetramethylpiperidine-1-oxyl radical-mediated oxidized (TEMPO)CNF hydrogel crosslinked with Ca^{2+} , Zn^{2+} , Cu^{2+} , Fe^{3+} , and Al^{3+} exhibited a storage modulus ranging from 0.2 to 2 kPa. Yang et al.²⁵ also investigated CNF-based composite hydrogels, finding that a 0.2–2 wt% TEMPO-CNF/Tetra-arm polyethylene glycol hydrogel displayed a storage modulus of 0.2–1 kPa. Yu et al.²⁶ investigated CNF/polypeptide hydrogel for the first time, analyzing their physical, chemical, and mechanical properties. The crosslinker was utilized at varied concentrations of 50 and 200 mM with the addition of only 12.5 mM of PLGA is Poly-L-lysine-co-L-glutamic acid (PLLGA) resulting in a storage modulus of 34 kPa for 1.91 wt% CNF/PLLGA hydrogel.²⁶ Their study demonstrated that the mechanical properties of CNF-containing hydrogels are heavily influenced by the crosslinking density. CNF-containing hydrogel, crosslinked with a poly-L-lysine-co-L-glutamic acid ($\text{PLL}_{80}\text{GA}_{20}$, PG) through hydrogen bonding, exhibited significantly improved mechanical strength. While synthetic corneal equivalents with corneal fibroblasts offer structural similarities to the original cornea, they are not clinically feasible due to

their limited thickness and complex fabrication methods. These materials have also been used to fabricate artificial corneas using techniques such as hydrogel fabrication, 3D printing,¹¹ and electrospinning.²⁷ However, their clinical use has been limited by postoperative difficulties, including host tissue rejection, vision obstructions, and persistent epithelial defects.²⁸

Over the last few decades, tissue engineering and regenerative medicine have provided alternative methods for forming tissues and organs to overcome the shortage of organ transplants. 3D printing of biomaterials offers a promising solution for producing human tissues and organs, potentially alleviating donor shortage. 3D bioprinting technology enables the fabrication of customizable corneal implants tailored to each patient's unique eye shape and size, increasing the likelihood of success and comfort.^{29,30} This adaptability of this technology allows for the integration of various biocompatible materials, such as hydrogels, biopolymers, and composites, facilitating the development of corneal implants that mimic the mechanical and optical properties of the natural cornea while promoting tissue integration and healing.¹⁸

However, there are limitations to previously reported scaffolds, including low transparency, reduced mechanical strength, high costs, prolonged testing before transplantation, susceptibility to tearing or wrinkling during suturing, and toxicity associated with poor material alignment.³¹ Therefore, developing alternative solutions for corneal transplantation, such as cell-based therapies and bioengineered constructs, is critical and urgent.³² Recently, alginate-based scaffolds have gained attention in tissue engineering due to their superior biocompatibility, biodegradability, non-toxicity, flexibility, and chelating ability. However, alginate alone has limitations, including high viscosity, low solubility, and poor degradability, which restrict its biological applications. To overcome these issues, various natural or synthetic biomaterials have been integrated into alginate structures. Alginate's excellent printability also makes it suitable for 3D printing applications.³³⁻³⁵

In this study, we developed a 3D-printed artificial cornea using 2 wt% sodium alginate (SA) and CNF composite scaffolds with dual crosslinking. During the fabrication of the hydrogel, two types of crosslinkers were employed: PG and calcium chloride (CaCl₂, CC), which were essential for maintaining the corneal shape following the 3D printing process. This innovative material demonstrates significant mechanical strength, low toxicity, and excellent hydrogel orientation. The PG was synthesized through a ring-opening polymerization method, and the composite hydrogel was fabricated. PG significantly improved the

mechanical strength of the hydrogels, with lysine playing a role in human protein synthesis and glutamate-promoting cell proliferation.³⁶ The potential of the synthesized polymer crosslinked SA/CNF composite hydrogel was evaluated by examining light transmittance, composite hydrogel orientation, and cytocompatibility. Since the mechanical properties of bio-ink were used for 3D printing cornea. Even at low concentrations, the 3D-printed PG-crosslinked hydrogel exhibited high mechanical strength, reaching a storage modulus of 2360 kPa.

2. Materials and methods

Triphosgene (98%, Sigma–Aldrich), benzyl amine (99%, Alfa Aesar), hydrobromic acid solution (33 wt% in acetic acid; 47 wt%, Sigma–Aldrich), L-glutamate(bz)-OH (≥99.0%, Sigma–Aldrich), L-lysine (Cbz)-OH (≥99.0%, Fluorochem), and SA (M_w 150–250 kDa) salt were obtained from Acros organics, and all solvents were purchased from Sigma–Aldrich. Detailed synthesis methods for L-glutamate N-carboxyl anhydride (BGNCA), L-lysine N-carboxyl anhydride (CBZNCA), and PG are provided in the Supplementary File as [Figures S1, S2, and S3](#), respectively. The PG was synthesized using the traditional ring opening polymerization method, with the procedure described in section [S1](#) of the Supplementary File. The preparation of bio-ink and printing procedure has been given in section [S1.5](#).

The synthesized BGNCA, CBZNCA, and PG were confirmed using differential scanning calorimetry (DSC), nuclear magnetic resonance spectroscopy (NMR), and Fourier transform infrared spectroscopy (FTIR) analysis. The fabricated hydrogels were investigated using polarized optical microscope (POM), scanning electron microscopy (SEM), and rheological analysis. Detailed methods of preparation and the information of the instruments used for every analysis are provided in Supplementary File, sections [S2](#) from [S2.1](#) to [S2.10](#)

3. Results and discussion

First, the BGNCA and CBZNCA were confirmed by DSC analysis presented in [Figure S4a](#), and then they were used to polymerize the PG. The surface functional group confirmed by the FTIR, as shown in [Figure S4b](#). The surface charges of the SA, CC, and PG were confirmed by the zeta potential before the gelation, and the data are presented in [Figure S4c](#) in Supplementary File with detailed explanation. [Figure S4d](#) showing the storage modulus of the control group hydrogel as SA and CC. The surface charge of SA was -32.76 mV, and that of the PG was 47.62 mV. The NMR representing the chemical structure of the monomers and polymers is shown in [Figure S5a–c](#) (in Supplementary File). The surface charge of SA was

-32.76 mV, and that of the PG was 47.62 mV. The hydrogels were prepared dual crosslinking based on their effective charge concentration of the crosslinker. According to our previous research, the toxicity of using PG with CC was lower at 25 mM effective charge concentration; therefore, in current research, we proposed the lowest molarity (effective charge concentration).²⁶ Concentrations of 6.25, 12.25, and 25 mM are the concentrations for the fabrication of hydrogels. To produce the hydrogel, we made the solutions and bio-ink, as depicted in Figure 1a, through the individual preparation of a 2 wt% SA aqueous solution and a CNF aqueous solution. Subsequently, we combined both composites and let them homogenize for 2 h. Following that, the composite solution was stirred at 300 rpm overnight. Aqueous solutions of the PG were prepared with effective charge concentrations of 6.25, 12.25, and 25 mM, respectively. The fabrication of hydrogels can be achieved through two distinct techniques: the dropped and co-injection methods. In the dropped method, the SA/CNF mixture was first mixed overnight, and then the crosslinker solution was carefully added dropwise. The ratio of SA/CNF solution to PG was maintained at 1:2. Although gelation initiates within a second, complete gelation necessitates an overnight immersion of the mixture in the crosslinker solution. Following the removal of the crosslinker solution, the hydrogels were placed in deionized water for an additional night under ambient conditions. This method, however, tends to result in uneven or bowl-shaped contact. In the co-injection method, a dual syringe system obtained from Nordon-medical was utilized, along with a 6 cm glass capillary

to ensure proper fiber alignment. One syringe was filled with the SA/CNF solution, while the other contained the crosslinker solution. The co-injection gels were created by simultaneously extruding both solutions through the dual syringe. The mixture was allowed to rest overnight within the capillary, resulting in a rod-like texture. The amount of CNF was 2 wt%, but the volume of the CNF optimized according to enhancement of the transparency of hydrogel. CNF is considered for its high fiber content, which results in minimal transparency attributed to its bundled structure. Consequently, after optimization with various volumes, 0.2 mL was selected for the hydrogel formation. The crosslinking mechanism during the hydrogelation is shown in Figure 1b(i). SA is the polymer chain included carboxyl groups (-COO⁻), which bind with divalent cations, such as Ca²⁺ in CC and NH₃⁺ in PG of the formation of a crosslinked network and gel. The crosslinking mechanism is shown in Figure 1b(ii). It can be observed that the SA provides the negative charges (COO⁻), while the PG acts as a crosslinker with positive charges (NH₃⁺), and CNF is used to align the hydrogel structure. Physical crosslinking takes place throughout the hydrogelation process by the dropped and co-injection methods. During the 3D printing process, dual crosslinking was employed, starting with physical crosslinking followed by chemical crosslinking. The second stage of crosslinking was achieved through the addition of Ca²⁺, resulting in covalent chemical bond formation, which provides chemical crosslinking as shown in Figure 1b(iii). The composition and nomenclature of the hydrogel on their effective charge concentrations are tabulated in Table 1.

Table 1. Composition of hydrogel with its nomenclature

Sample name	Crosslinker	Sample code	Effective charge concentration (mM) of crosslinker
PLL ₈₀ GA ₂₀	-	PG-1	6.25
		PG-2	12.50
		PG-3	25
CNF	CaCl ₂	CNF/CC-1	6.25
		CNF/CC-2	12.50
		CNF /CC-3	25
CNF	PLL ₈₀ GA ₂₀	CNF/PG-1	6.25
		CNF/PG-2	12.50
		CNF/PG-3	25
SA/CNF	PLL ₈₀ GA ₂₀	SA/CNF/PG-1	6.25
		SA/CNF/PG-2	12.50
		SA/CNF/PG-3	25
3D-printed SA/CNF	PLL ₈₀ GA ₂₀ /CaCl ₂	SA/CNF/PG/CC-1	6.25
		SA/CNF/PG/CC-2	12.50
		SA/CNF/PG/CC-3	25

Abbreviations: CC: calcium chloride; CNF: cellulose nanofibers; PG: poly-L-lysine-co-L-glutamic acid (PLL₈₀GA₂₀); SA: sodium alginate.

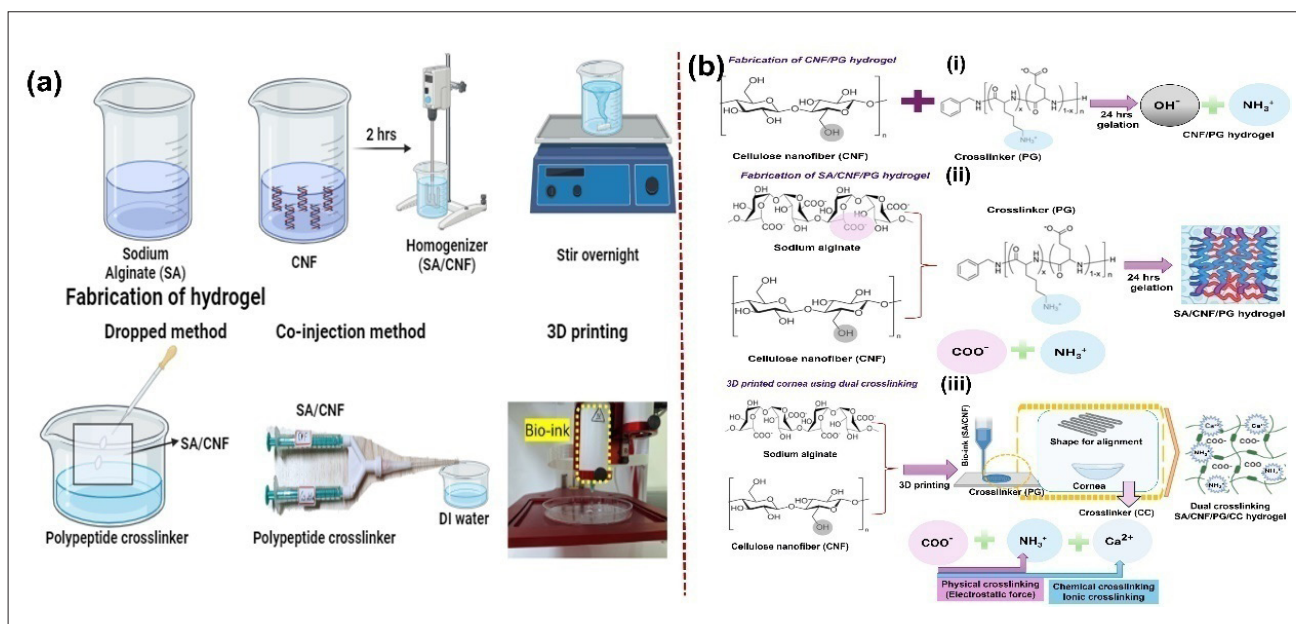


Figure 1. Preparation method of bio-ink with crosslinking mechanism before and after 3D printing. (a) Schematic for the preparation of solutions and bio-inks for the fabrication of hydrogel. (b) Crosslinking mechanism of the CNF/PG hydrogel (i), crosslinking mechanism of the SA/CNF/PG hydrogel (ii), 3D -printed dual crosslinking mechanism of the SA/CNF/PG/CC hydrogel (iii). Abbreviations: CC: calcium chloride; CNF: cellulose nanofibers; PG: poly-L-lysine-co-L-glutamic acid (PLL₈₀GA₂₀); SA: sodium alginate.

The mechanical properties of the hydrogels are presented in Figure 2a–d, with detailed parameters tabulated in Table 2, including the water content calculated by Equation S1 (see Supplementary File). All hydrogels demonstrated a water content exceeding 96%, indicating their hydrophilic nature and potential suitability for tissue engineering applications. Figure 2a shows the viscoelastic behavior of the hydrogels, where higher viscosity indicates increased crosslink density. In contrast, decreased viscosity suggests fewer crosslinks, which allows for easier flow. Fewer crosslinks reduce the interaction between polymer chains, increasing their mobility and lowering internal friction. Conversely, more crosslinks restrict the movement of polymer chains, increasing internal friction and, as a result, viscosity. The compositions of CNF/CC-1, CNF/CC-2, CNF/CC-3, CNF/PG-1, CNF/PG-2, and CNF/PG-3 displayed good viscosity, but printing was challenging due to the bundle structure of CNF, which caused clogging in the 3D printer needle. To address this, SA was introduced into the composite hydrogel, resulting in good printability with high viscosity. The SA/CNF/PG-1, SA/CNF/PG-2, and SA/CNF/PG-3 exhibited higher viscosity of 657.12 ± 12.89 Pa·s, 987.10 ± 10.21 Pa·s, and 1064.21 ± 40.12 Pa·s, respectively. Figure 2b presents the storage modulus of the fabricated hydrogel, which depends on the crosslink density and mechanism. The values of the storage modulus of CNF/CC-1, CNF/CC-2, and CNF/CC-3 were 4.74 ± 0.26 kPa, 8.86 ± 1.46 kPa, and 20.07 ± 1.33 kPa, respectively.

For the PG-containing crosslinker (SA/CNF/PG-1 to SA/CNF/PG-6), the storage modulus ranged from 19.44 ± 0.53 kPa to 87.18 ± 0.21 kPa, showing higher values than those with CC crosslinker. To investigate and confirm the effect of enhanced ionic crosslinking on mechanical strength, as shown in Figure S4d with corresponding values tabulated in Table S1, the mechanical properties of hydrogel can be significantly enhanced by increasing the degree of ionic crosslinking between SA and CC. The storage modulus can be enhanced through the precise regulation of the concentrations of Ca^{2+} as effective charge concentrations (6.25, 12.25, and 25 mM). The storage modulus of the produced hydrogel depends upon the crosslink density and mechanism. The storage modulus values for SA/CC-1, SA/CC-2, and SA/CC-3 were 18.31 ± 1.39 kPa, 38.01 ± 0.89 kPa, and 42.76 ± 0.52 kPa, respectively. The dual crosslinking mechanism, involving ionic interactions between CNF and CC and electrostatic interactions between CNF and PG, significantly enhanced the mechanical strength of hydrogen. In this process, Ca^{2+} from CC interact with negatively charged hydroxyl groups on CNF, forming ionic bonds that strengthen and stabilize the CNF network. Additionally, electrostatic interactions between CNF and PG further contribute to crosslinking. The PG participates in the network formation; however, its contribution to the storage modulus is far less pronounced than ionic crosslinking provided by Ca^{2+} . Whereas PG may participate in some physical interactions with both

the alginate and CNF components, these interactions are much weaker than the ionic bonds formed by the Ca^{2+} . Therefore, the substantial improvement in the storage modulus observed in the SA/CNF/Pg/CC system cannot be explained solely by the presence of Pg. The main factor contributing to the increased storage modulus in the SA/CNF/Pg/CC systems is the presence of Ca^{2+} , which provides ionic crosslinks within the SA matrix. These CC are believed to form a complex network of strong ionic bonds with the guluronic acid in SA, significantly reinforcing the rigidity of the gel network. When the Ca^{2+} crosslink with the SA chains in the SA/CNF/Pg/CC system, they form a so-called “egg-box” structure with the G-blocks, resulting in a compact and highly crosslinked network.³⁷ This increased crosslinking decreases the moving ability of the polymer chains, leading to greater stiffness and a higher storage modulus. In contrast, the SA/CNF/Pg system, lacking Ca^{2+} , is stabilized solely through weaker physical interaction among SA, CNF, and Pg. The absence of ionic crosslinking provided by Ca^{2+} results in a more flexible polymer network with reduced rigidity, leading to a lower storage modulus in comparison to GA/CNF/(EP-g-GMA). While the Ca^{2+} in the SA/CNF/Pg/CC material offers multiple ways to enhance the storage modulus, such as forming a denser network structure and increasing the crosslinking density. Therefore, the ionic crosslinking process develops a more rigid and densely packed structure, restricting the mobility of polymer chains and CNFs within the matrix. As a result, the material exhibits greater resistance to deformation under shear stress, leading to an improved storage modulus. Calcium ions significantly increase the crosslinking density within the SA matrix, directly enhancing its mechanical strength and ability to store elastic energy during deformation. This explains why the storage modulus is much higher in SA/CNF/Pg/CC than in SA/CNF/Pg.

Figure 2c shows the evidence of the higher storage modulus of the 3D-printed SA/CNF-containing hydrogels, where dual crosslinking hydrogels improved mechanical strength by more than two orders of magnitude with the same concentration as Pg crosslinkers. The SA/CNF/Pg/CC-1, SA/CNF/Pg/CC-2, and SA/CNF/Pg/CC-3 compositions exhibited storage modulus of 2360 ± 125.78 kPa, 4065 ± 109.23 kPa, and 7065 ± 129.32 kPa, respectively. These behaviors could be attributed to the molecular weight and chemical composition of Pg. First, due to their polymeric structure, the size of Pg is more than ten times larger than metal cations, contributing to stronger interactions. Second, hydrogen bond provides an additional contact force between SA/CNF and Pg. The carbonyl groups on Pg act as hydrogen bond acceptors, interacting with the hydroxyl groups of CNF, while the

amine groups on Pg function as hydrogen bond donors, interacting with carbonyl or hydroxyl groups. These interactions enable Pg to efficiently connect SA/CNF, thereby increasing the stiffness of the network. Figure 2d illustrates the curve between storage modulus and oscillation strain in compression mode, demonstrating the viscoelastic properties of hydrogel. Various techniques have been developed for the fabrication of scaffolds, but most of these techniques are not very efficient due to complications in fabricating scaffolds that allow 3D healing and vascularization of blood vessels inside the scaffold.³⁸ The degradability of the scaffold material denies the need for its post-healing removal and hence negates the side effects related to residual material in the host. Yue et al.³⁹ reported the cellulose nanofibrils and SA as compound matrix based on double crosslinking strategy and introduced the boric acid/ Ca^{2+} ; through this method, they found the mechanical properties of 22.8 kPa. Zander et al.⁴¹ have demonstrated that PEG-based hydrogels exhibit storage moduli from 20,000 to 28,000 Pa. *In vivo* studies, for example, illustrated that the addition of cellulose nanocrystals to maleic anhydride-grafted poly(lactic acid) scaffolds resulted in scaffolds with compressive strengths in the range of 0.025 and 0.4 MPa with elastic moduli in the range of 0.04 and 0.15 MPa.⁴² Kim et al.⁴³ fabricated composite scaffolds using polymeric materials with nano-hydroxyapatite. The prepared scaffold improved mechanical properties, such as compressive modulus at 4.5 MPa and tensile modulus at 27 MPa. The sample with 20 wt% hydroxyapatite/PLGA exhibited better mechanical properties, compressive strength of 2.31 MPa,⁴⁴ a very good viability of osteoblasts, and enhanced stability *in vitro* degradation. Significantly, the mass loss for the maleic anhydride-grafted poly(lactic acid) scaffold after one month was 46.5 wt%, while that for the cellulose nanocrystal-PLA scaffold was 40 wt%. According to the literature, our SA/CNF scaffolds establish the advantage of the usage of exclusively biocompatible and biodegradable materials, reducing the possibility of an inflammatory or immune response in relation to their synthetic counterparts. The environment, which provides ground totally conducive to the growth and regeneration of cells in terms of performance, is due to the biocompatibility of SA, in addition to the minimum molarity of Pg that possesses 2,360 kPa of mechanical strength, along with degradation of 35.9% in 28 days. The fibrous structure of the corneal cells possibly matches or even outperforms the performance of collagen-based scaffolds conventionally used. The SA/CNF scaffold, in summary, presently shows a very good balance of transparency, strength, and biocompatibility, with much promise in comparison to other test materials in corneal tissue engineering.

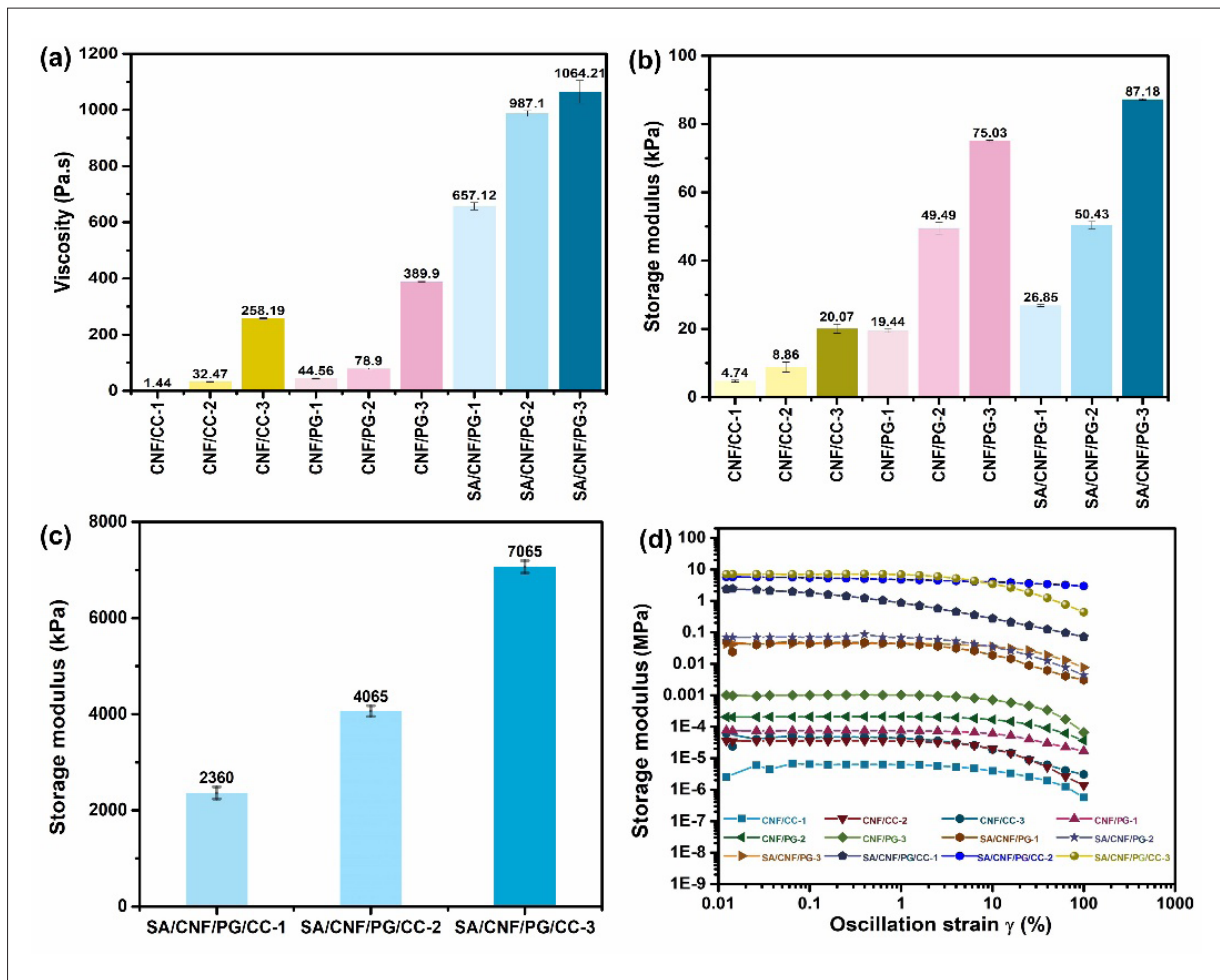


Figure 2. Mechanical properties of the hydrogel before and after printing. (a) Viscosity of the hydrogel. (b, c) Storage modulus of the hydrogel (b) and the 3D-printed cornea (c), respectively. (d) Viscoelastic behavior of the hydrogel and 3D-printed cornea. Abbreviations: CC: calcium chloride; CNF: cellulose nanofibers; PG: poly-L-lysine-co-L-glutamic acid (PLL₈₀GA₂₀); SA: sodium alginate.

Table 2. Mechanical properties of composite hydrogel and 3D-printed hydrogel

Sample code	Viscosity (Pa·s) (n = 3)	Water content (wt%)	Storage modulus G' (kPa) (n = 3)
CNF/CC-1	1.44 ± 0.45	98.32 ± 0.14	4.74 ± 0.26
CNF/CC-2	32.47 ± 1.4	97.10 ± 0.20	8.86 ± 1.46
CNF/CC-3	258.19 ± 1.78	96.18 ± 0.70	20.07 ± 1.33
CNF/PG-1	44.56 ± 1.1	98.67 ± 0.20	19.44 ± 0.53
CNF/PG-2	78.90 ± 1.9	98.42 ± 0.43	49.49 ± 1.69
CNF/PG-3	389.90 ± 2.1	97.83 ± 0.50	75.03 ± 1.34
SA/CNF/PG-1	657.12 ± 12.89	97.09 ± 0.49	26.85 ± 0.28
SA/CNF/PG-2	987.10 ± 10.21	98.31 ± 0.12	50.43 ± 1.04
SA/CNF/PG-3	1064.21 ± 40.12	97.49 ± 0.25	87.18 ± 0.21
SA/CNF/PG/CC-1	-	97.31 ± 0.17	2360 ± 125.78
SA/CNF/PG/CC-2	-	96.09 ± 0.48	4065 ± 109.23
SA/CNF/PG/CC-3	-	97.67 ± 0.31	7065 ± 129.32

Abbreviations: CC: calcium chloride; CNF: cellulose nanofibers; PG: poly-L-lysine-co-L-glutamic acid (PLL₈₀GA₂₀); SA: sodium alginate.

The alignment of the fabricated hydrogels is presented in Figure 3a–l. A polarized microscope was used to observe the fibrous hydrogel, and the alignment was measured in two modes: (i) cross-polar, and (ii) cross-polar + compensator, where the polarized and analyzer are perpendicular to each other so that birefringent phases can be identified. The image resembles a standard optical microscope when the polarizer and analyzer are aligned in the same polarization direction. The mode reveals the shape and density variations between different phases of the hydrogel.⁴⁵ When a compensator is added, birefringent phases with varying orientations display different colors. In Figure 3a–b, the CNF/PG-1 hydrogel fabricated using the dropped method shows a fibrous structure under cross-polar light, but no orientation was observed after adding the compensator, as indicated by the blue and orange colors in the image. Figure 3c–d shows a sample fabricated by the co-injection method, displaying a thin and fibrous morphology under cross-polar light. After adding the compensator, an orange color was observed,

indicating the hydrogel's alignment in the southeast direction and confirming a well-aligned hydrogel structure. Figure 3a demonstrates that the hydrogels containing SA/CNFs, made using the dropped method, exhibited a non-uniform microstructure under cross-polar light. This uneven surface may result from the instability caused by the dropped method and the chemical structure of the PG, which contributed to hydrogen bonding. When the compensator was added (Figure 3b), the hydrogel exhibited birefringence, but no clear alignment was observed, as indicated by the blue and orange colors typically used to label orientations (northeast-southwest or northwest-southeast). In Figure 3e–f, the SA/CNF/PG-1 hydrogel, fabricated using the co-injection method, shows an uneven and thick morphology under cross-polar light, likely due to the higher viscosity of SA-containing hydrogel after gelation. Although no orientation was observed in the dropped method, the fibrous structure was evident. Figure 3g–h exhibits the aligned hydrogel produced using the co-injection method, showing a rod-like structure and

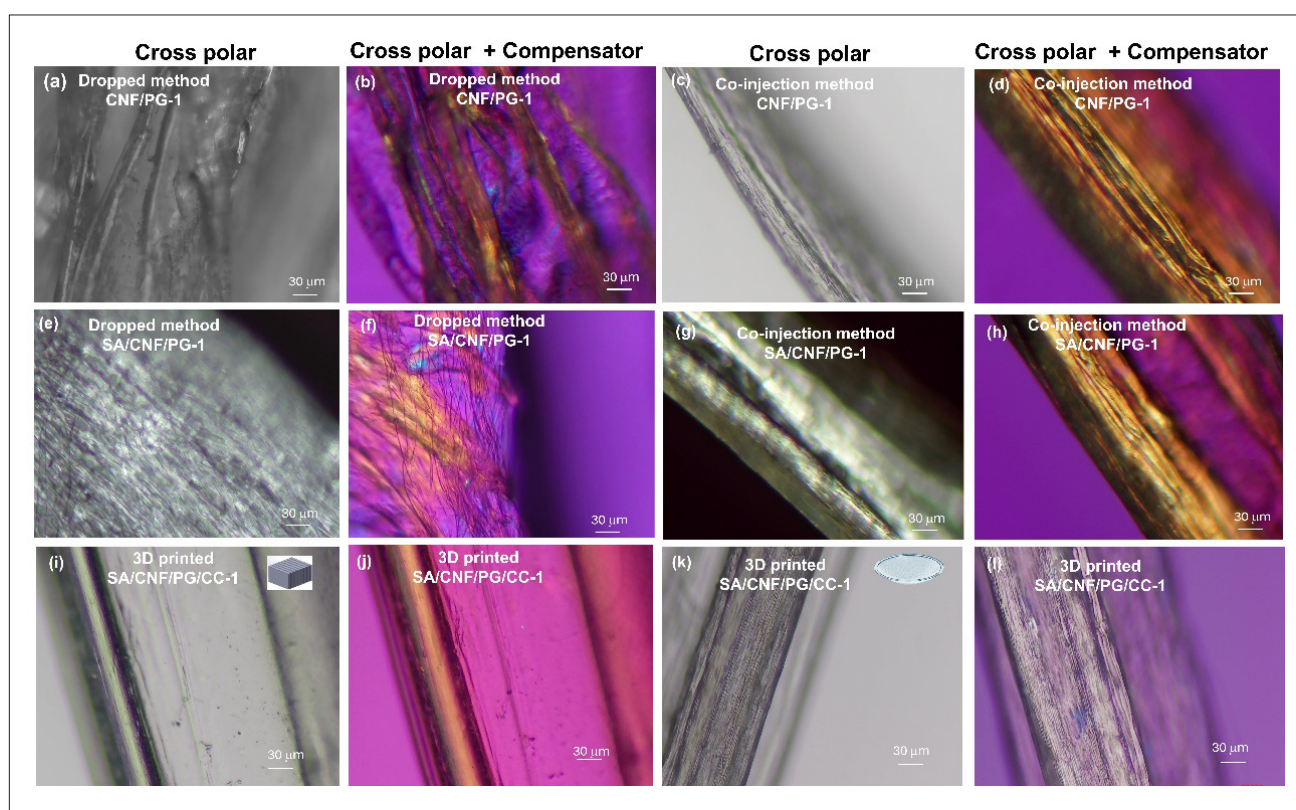


Figure 3. POM images to study orientation. (a) Cross-polar CNF/PG-1, and (b) cross-polar + compensator CNF/PG-1 by dropped method. (c) Cross-polar CNF/PG-1, and (d) cross-polar + compensator CNF/PG-1 by co-injection method. (e) Cross-polar SA/CNF/PG-1, and (f) cross-polar + compensator SA/CNF/PG-1 by dropped method. (g) Cross-polar SA/CNF/PG-1, and (h) cross-polar + compensator SA/CNF/PG-1 by co-injection method. (i) Cross-polar SACNF/PG/CC-1, and (j) cross-polar + compensator SA/CNF/PG/CC-1 by 3D printing of hydrogel in parallel shape. (k) Cross-polar SA/CNF/PG/CC-1, and (l) cross-polar + compensator SA/CNF/PG/CC-1 by 3D printing of hydrogel in cornea shape. Magnification: $\times 100$. Abbreviations: CC: calcium chloride; CNF: cellulose nanofibers; PG: poly-L-lysine-co-L-glutamic acid ($PLL_{80}GA_{20}$); SA: sodium alginate.

uniformity in the fiber-containing hydrogel. This material holds significant promise for future applications in tissue engineering; it demonstrates how an effectively high-aspect ratio of CNF can align during the extrusion process. Figure 3i–j shows the 3D-printed SA/CNF/PG/CC-1 hydrogel in a rectangular shape, confirming the hydrogel’s alignment and even morphology after the printing process. Finally, Figure 3k–l displays the 3D-printed cornea hydrogel undercross-polar mode and cross-polar + compensator modes, revealing a very thin, uniform hydrogel with good orientation. These results are promising for cornea applications, as the hydrogel provides high mechanical strength, and replicates the lamellar structure present within the cornea.

The most important property of the cornea is its transparency, as it refracts light onto the lens before it reaches the retina. To evaluate this property in the

hydrogel-based 3D-printed cornea, the transmittance of PG solutions (6.25, 12.25, and 25 mM), CNF, and SA were measured both before and after gelation. Initially, the transparency was about 90% in the 500–700 nm range before the gelation. However, the transparency reduced because of the aggregation of CNF after the gelation, which is highly fibrous and can reduce transparency. The transmission spectrum is recorded between 300 and 700 nm, as shown in Figure 4a–b. Based on the transmittance of 6.25, 12.25, and 25 mM, the 6.25 mM crosslinker concentration was selected for the 3D printing. As shown in Figure 4b, the transmittance of the SA/CNF composite is more than 90% in the visible range (400–700 nm). Figure 4c illustrates the transmittance of the 3D-printed artificial cornea, which achieved over 82% transparency in the visible range, with 86% transmittance at 550 nm. According to the previous literature^{46–53} (Figure 4d), the transparency of the 3D-printed cornea has been improved

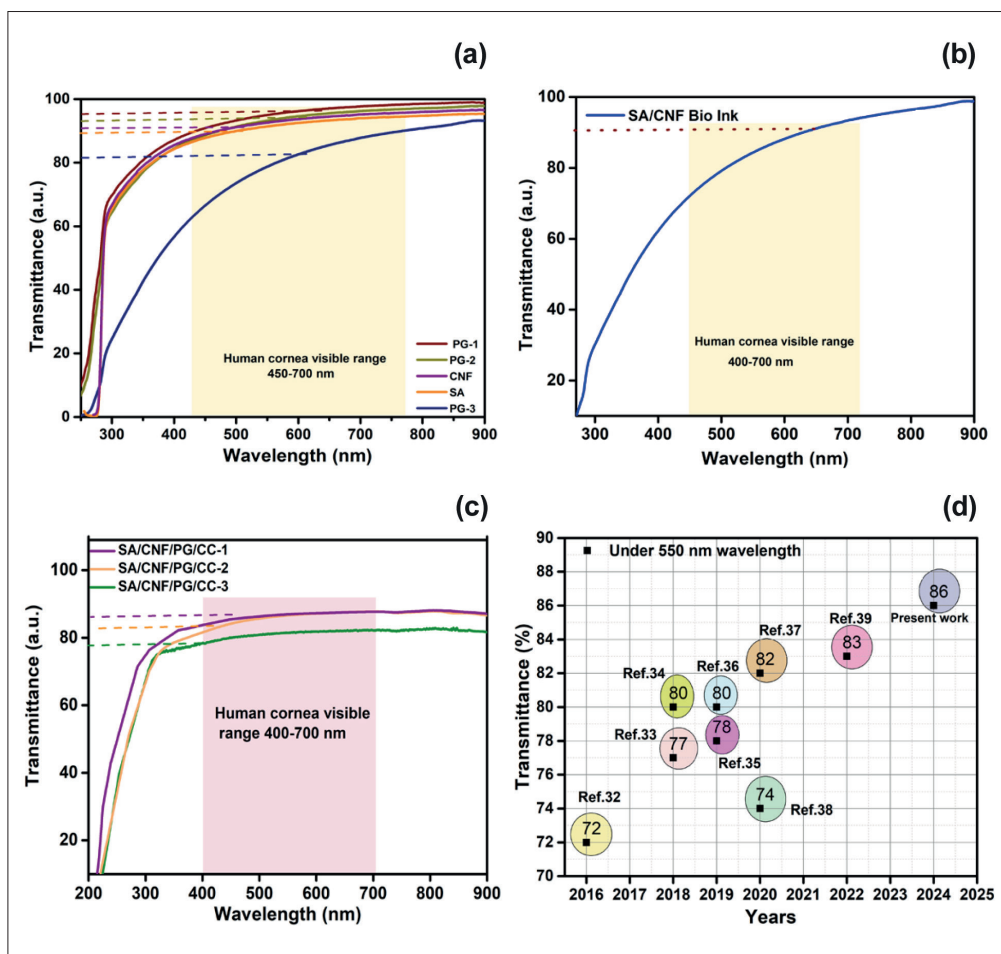


Figure 4. Optical properties of hydrogel before and after printing. (a–c) Transmittance of the solution before printing (a), the SA/CNF composite (b), and the printed artificial cornea (c). (d) Reported transmittance value at 550 nm from the literature.^{xx} Abbreviations: CC: calcium chloride; CNF: cellulose nanofibers; PG: poly-L-lysine-co-L-glutamic acid (PLL₈₀GA₂₀); SA: sodium alginate.

by this formulation. It has been found that the optical transmittance in human cornea tissue typically ranges from 50% to 60% between 400 and 550 nm and from 60% to 75% between 550 and 700 nm.⁵⁴ In the 300–400 nm range, which corresponds to the UVA and UVB regions, transparency decreases, resulting in lower transmittance.

The bio-ink preparation involves two steps. First, an aqueous solution of SA (3 mL) and CNF (0.8 mL) was mixed at room temperature using a magnetic stir until completely dissolved, resulting in a homogeneous solution. In the second step, the PG aqueous solution was prepared. The compositional ratios between SA/CNF and PG were 1:2. The printing specifications for the parallel-shaped mold were optimized to ensure proper alignment of the hydrogel. After printing, a 6.25 mM CC solution was applied dropwise onto the printed structure. A dual crosslinking step was utilized during the 3D printing to maintain the structure integrity of the cornea shape. The surface morphology of 3D-printed cornea hydrogel was analyzed by SEM. For this analysis, a dried cornea-shaped hydrogel was used. As shown in Figure 5a–c, the surface shows the fibrous structure with uniformity, resulting in a high crosslink density. This uniform morphology was achieved due to the fibrous bio-ink. Figure 5d–f further

demonstrates the alignment of the printed hydrogel with a fibrous structure. It also shows the 3D-printed cornea shape without fibrous material. The control group SA/PG/CC-1 exhibited no uniformity after printing, highlighting the importance of the fibrous material in achieving the desired structural characteristics, as shown in Figure S6a–c. The transparency and shape of the cornea are shown in Figure S6d.

Cytocompatibility of the SA/CNF/Pg/CC-1, SA/CNF/Pg/CC-2, and SA/CNF/Pg/CC-3 compositions was studied, which were selected based on the mechanical properties of the hydrogels. PC-12 cells were cultured, and live dead cells assays were performed after 7 days. The detailed protocol of the cytotoxicity and cell viability given in section S2.8 (see Supplementary File). The cytotoxicity was performed by using Live/Dead assay on day 7 after seeding cells on the fabricated hydrogel. Two staining solutions, calcein-AM and ethidium homodimer-1 (EthD-1), were used for the Live/Dead assays, respectively. The green-colored cells indicate the live cells and the red ones are the dead cells. As shown in Figure 6a–f, the cornea is nontoxic at both low and high molarity of the PG. Furthermore, the dual crosslinking method enhanced cell adhesion due to the hydrogel's increased stability in

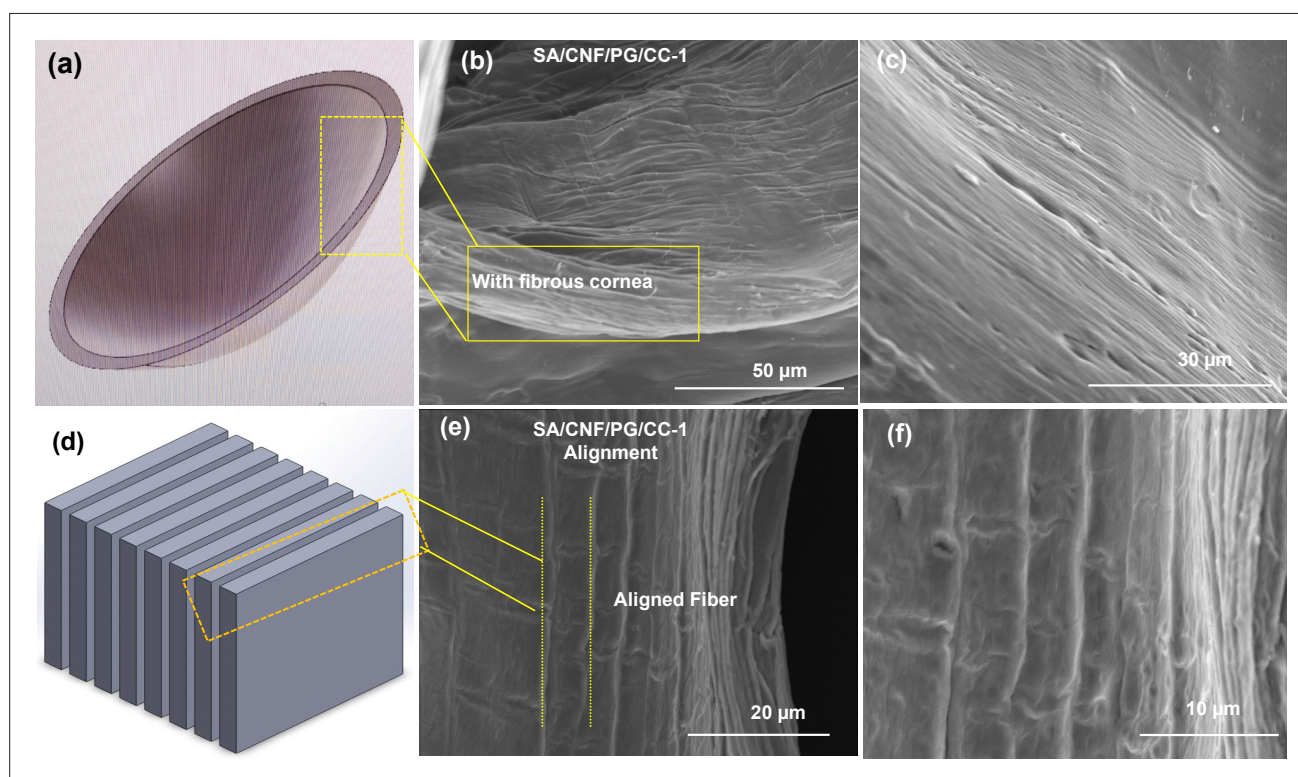


Figure 5. Surface morphology of the 3D-printed cornea and aligned shape. (a–c) Surface morphology of the 3D-printed cornea at 50 μm scale and 30 μm scale. (d–f) Aligned fibrous structure of the 3D-printed hydrogel at 50 μm scale and 30 μm . Magnification: b (x1000), c (x2500), e (x2000), f (x3000). Abbreviations: CC: calcium chloride; CNF: cellulose nanofibers; PG: poly-L-lysine-co-L-glutamic acid (PLL₈₀GA₂₀); SA: sodium alginate.

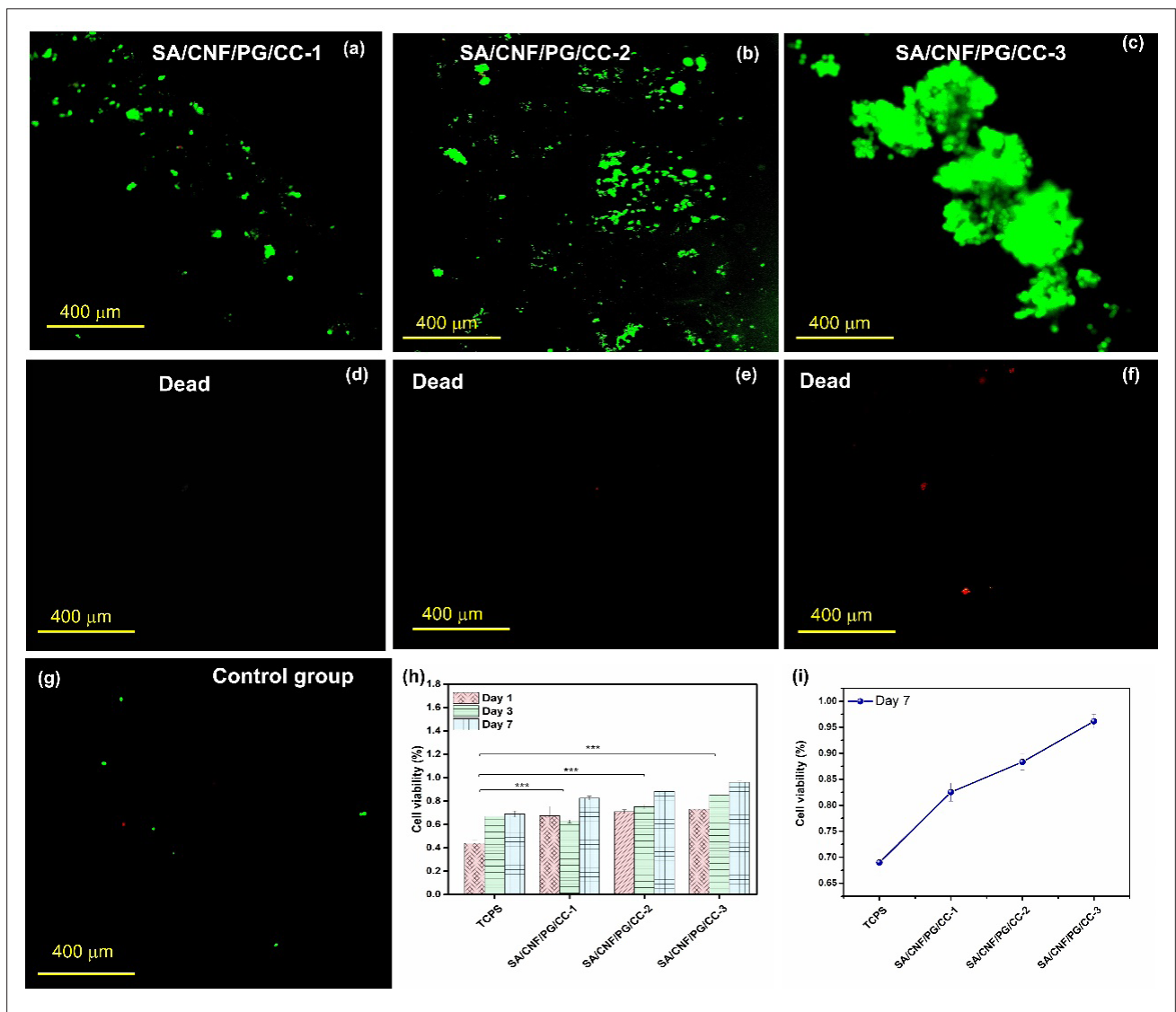


Figure 6. Cell culture studies. (a–c) Live cell study of the SA/CNF/Pg/CC-1, SA/CNF/Pg/CC-2, and SA/CNF/Pg/CC-3 hydrogels. (d–f) Dead cell study of the SA/CNF/Pg/CC-1, SA/CNF/Pg/CC-2, and SA/CNF/Pg/CC-3 hydrogels. (g) Overlay of the control group. (h) Cell viability study of SA/CNF/Pg/CC-1, SA/CNF/Pg/CC-2, and SA/CNF/Pg/CC-3 hydrogels on days 1, 3, and 7, where $P < 0.001$. (i) Comparison of cell viability of SA/CNF/Pg/CC-1, SA/CNF/Pg/CC-2, and SA/CNF/Pg/CC-3 hydrogels on day 7. Abbreviations: CC: calcium chloride; CNF: cellulose nanofibers; PG: poly-L-lysine-co-L-glutamic acid (PLL₈₀GA₂₀); SA: sodium alginate.

phosphate-buffered saline (PBS). The hydrogel, containing PG crosslinkers, plays various critical roles in cell culture, particularly in supporting cell growth, differentiation, and function. The PG is composed of glutamate and lysine. Glutamate, an amino acid, influences various aspects of cellular metabolism and function, while lysine is essential to produce antibodies and other immune proteins, aiding immune cell cultures in generating these crucial proteins. Additionally, cell adhesion was improved by the incorporation of PG, which enhanced the interaction between the scaffold and the cells, providing a more favorable environment for cell attachment and proliferation.

Based on the results, we conclude that the cornea is biocompatible at the highest effective PG concentration of 25mM. The images show less dead cells because the PC12 cell line employed in this research is derived from a rat adrenal tumor called a pheochromocytoma, which is less vulnerable to cell death. These cells thrive in a controlled environment to grow, for instance, in a high-glucose RPMI-1640 medium supplemented with horse serum and fetal bovine serum. Optimal culture conditions, such as a temperature of 37°C and a CO₂ concentration of 5% along with saturating humidity composition, contribute to enhanced cell survival and decreased cell death rates

in laboratory settings. The cells tend to form clusters and exhibit viability under confluence levels over extended periods of time. When utilizing hydrogel after a week's time frame, for instance, a noticeable decrease in cell mortality would be observed, which sustains their longevity. A not-too-crowded environment, with cells in the culture setting and space and resources for them to grow without feeling overwhelmed or strained, results in a decrease in cell death rates. [Figure 6g](#) shows the images of the control group obtained from each specimen ($n = 3$), which were used for analysis and compared to those cultured on tissue culture polystyrene (TCPS) as a control. The overlay image shows the adhesion of cells with live and dead cells. In general, two ways prevail to categorize a material as low-cytotoxic or biocompatible. The first condition is that the cell viability needs to be over 1 on days 3 and 7. The second condition is that the percentage of live cells should be more than 50%. Generally, low cytotoxicity is observed in the various combinations of synthetic polymers such as the hydrogels with SA/PG/CNF/CC-1 prepared via dual crosslinking. Results from the alamarBlue cell viability test indicate that these constructed objects, through the gel, increased the viability rate from 67% on day 1 to 82% for the SA/PG/CNF/CC-1 hydrogel, from 70% to 88% for the SA/PG/CNF/CC-2 hydrogel, and from 73% to 96% for the SA/PG/CNF/CC-3 hydrogel, with the rate calculated using [Equation S2](#) (see Supplementary File). In contrast, hydrogels produced with reduced concentration also evidenced the fact that, due to over 50% cell viability, they boast higher cell viability rates compared to others. The ANOVA test showed the most considerable differences in cell density among the three timepoints recorded in this study, *i.e.*, a significant increase of live cell density from 67% on day 3 to 96% on day 7 for SA/PG/CNF/CC-1, SA/PG/CNF/CC-3, and SA/PG/CNF/CC-3 hydrogels, with respect to control samples ([Figure 6h](#)). The SA/PG/CNF/CC-1 hydrogel featured a 67% increase in cell density with respect to control ($P < 0.001$), and the SA/PG/CNF/CC-3 hydrogel showcased a 96% increase with respect to control ($P < 0.001$). From the ANOVA test results, the P -values recorded are less than 0.001. The concentration of PG is important for affecting cell viability in the hydrogel lattice, possibly through elastic modulus and cell adhesion to the matrix. The Live/Dead cell viability assay results further confirm the observations made based on the alamarBlue staining results, indicating a high density of live cells, with a 96% increase of live cell number in the SA/CC/PG/CNF-3 hydrogel, suggesting that 25 mM of SA/CC/PG/CNF-3 is not only cytocompatibility but also non-toxic to the material. However, contrary to the alamarBlue findings, Live/Dead assay showed that in crosslinked PG hydrogels, cell viability was significantly affected by PG concentration since only the hydrogels containing the

least amount of PG were less attached to the cells. Based on the cell viability study by Paul et al.⁵⁵ that poly-L-lysine is somewhat toxic to the cells and mammals, we argue that very low levels of lysine prove biocompatible for the cells. Also, Paul et al.⁵⁶ demonstrated that culturing on variable cationic polyelectrolyte concentration-coated surfaces would trigger the initiation of apoptosis in HepG2 cells. [Figure 6i](#) shows that the cell viability increased with the molarity of PG in the SA/CNF/PG/CC-1, SA/CNF/PG/CC-2, and SA/CNF/PG/CC-3 hydrogels on day 7.

The degradation study was conducted over 1.524 days using dried hydrogel scaffolds, and the detailed explanations are presented in section [S2.9](#) (see Supplementary File). [Figure 7a](#) displays the degradation rates of scaffolds containing the PG crosslinker. The data revealed that CNF/PG-1, CNF/PG-2, and CNF/PG-3 hydrogels exhibited significant weight loss within a shorter duration. Specifically, the CN/PG-1 degraded by 14%, while the SA/CNF/PG/CC-1 hydrogel at same molarity degraded by only 7.87% after 3 days. This difference is attributed to the higher crosslink density in the SA/CNF/PG/CC-1 hydrogel than in the CNF-based hydrogel. The CNF/PG-1 hydrogel, being softer and thinner, degraded more rapidly compared to the SA-based hydrogel.

The degradation curve shows that the SA/CNF/PG/CC-1 composite hydrogel degraded by 28% after 21 days, while CNF/PG-1 degraded by 45%, and the degradation rate was calculated by [Equation S3](#). Previous studies have reported that the SA containing hydrogel typically degraded by 35.9%.⁵⁷ The results indicate that incorporating SA can effectively reduce the degradation rate of porous scaffolds, likely due to the increased crosslink density and the formation of an interpreting network. [Figure 7b, c, e, and f](#) show the surface morphology of the hydrogel before and after degradation, clearly illustrating the degradation of the scaffold. [Figure 7d](#) presents a comparative analysis of the degradation percentages. The SA/CNF scaffold primarily comprises natural biocompatible polymers, significantly reducing the risk of immune rejection or inflammatory reactions. This unique attribute makes it suitable for long-term tissue integration in corneal implants and tracheal stents. Another important advantage is their biodegradability; the scaffold degrades progressively over time as it is replaced by host tissue, eliminating the need for surgical removal, both for tracheal stents and potentially for corneal applications. The intrinsic properties of nanofibers, including their antimicrobial action and controlled degradation, can reduce post-surgical infection or other complications often associated with synthetic scaffolds. However, there are limitations to consider. The structural stability of the SA/CNF ink could present a disadvantage. While the scaffold initially exhibits

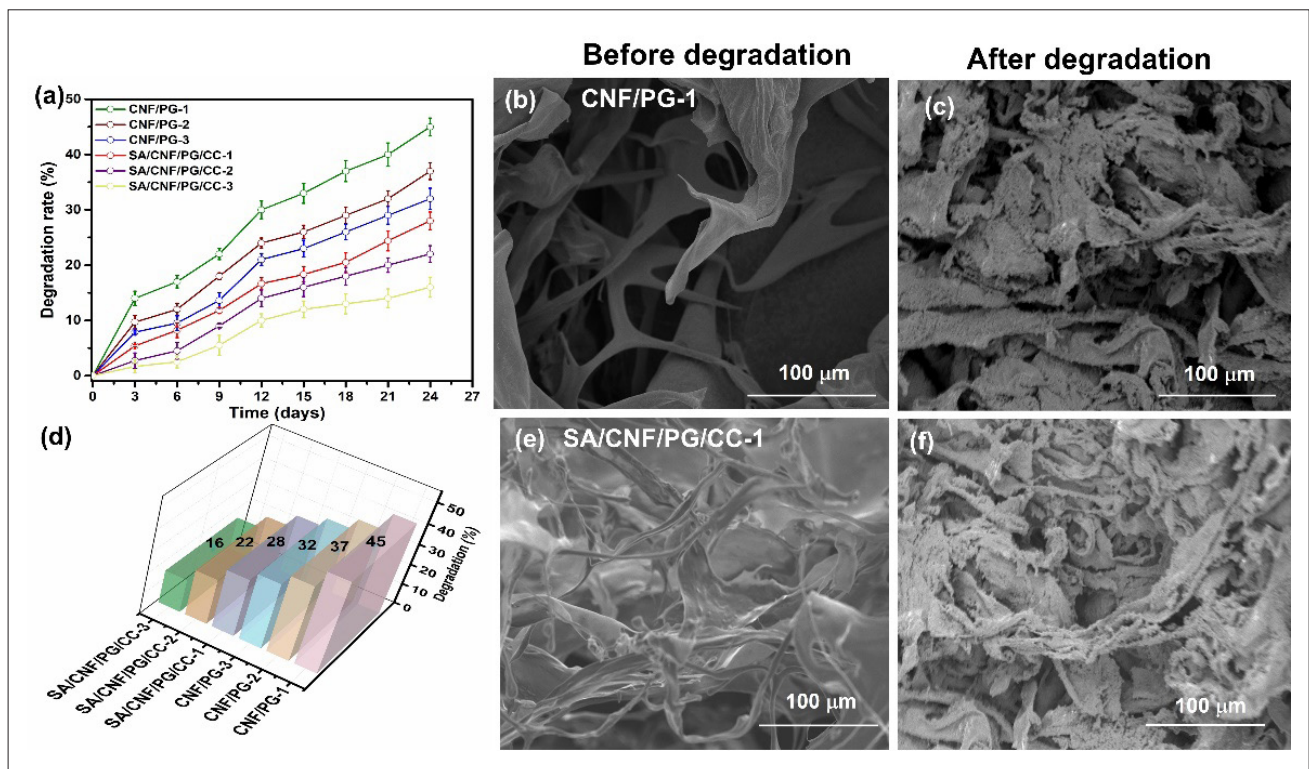


Figure 7. Degradation studies (a) Degradation study of CNF/PG-1, CNF/PG-2, CNF/PG-3, SA/CNF/PG/CC-1, SA/CNF/PG/CC-2, and SA/CNF/PG/CC-3 hydrogels over 3, 6, 9, 12, 15, 18, 21, and 24 days. (b,c) Surface morphology of CNF/PG-1 before (b) and after degradation (c), respectively. (d) Comparison of the hydrogel's degradation level. (e, f) Surface morphology of SA/CNF/PG/CC-1 before (e) and after degradation (f), respectively. Abbreviations: CC: calcium chloride; CNF: cellulose nanofibers; PG: poly-L-lysine-co-L-glutamic acid (PLL₈₀GA₂₀); SA: sodium alginate.

a good balance of flexibility and strength, questions may arise regarding its durability in mechanically demanding environments, such as the interior of the trachea, over extended periods. Additionally, for corneal applications, the sustainability of performance during continuous eye movements and exposure to tears and light may pose further challenges.

Rheological tests and preliminary degradation results gave promising signs for an assurance in stability and integrity of the SA/CNF artificial cornea scaffold. Degradation studies have been performed in which, under controlled conditions, the SA/CNF scaffold indeed degrades, an important aspect of its function in the healing of the cornea. Given the seemingly promising initial results on the SA/CNF artificial cornea scaffold, our current understanding of this material holds great promise for future clinical trials.

The cornea is a highly hydrated fibrous tissue, containing about 78% water. Individual collagen fibrils have a diameter in the range of 22.5–35 nm, with inter-fibril spacing of about 41.5 nm. The collagen fibrils in one lamella lie orthogonally to adjacent lamellae. This precise arrangement and hydration give the cornea particular

mechanical strength, allowing it to refract light by 80%. In one of the studies done on normal subjects, Young's modulus was stated to be 0.29 ± 0.06 MPa. In this study, we successfully attained the values required for functionality of a native cornea, as per the literature currently available concerning this subject.⁵⁸

4. Conclusion

In this study, we successfully synthesized the PG with a molecular weight of 47 kDa and developed a fibrous bio-ink (SA/CNF) that achieved high mechanical strength, exhibiting a storage modulus of 2360 kPa after dual crosslinking. The initial transparency of the bio-inks was over 92%, and this was maintained at 86% after 3D-printing the cornea. The dual crosslinking process significantly improved both the storage modulus and degradation rate of the hydrogel. Cell culture results demonstrated that the fabricated hydrogel at both low and high molarity exhibited good cytotoxicity and excellent biocompatibility. Additionally, cell adhesion improved due to PG enhancing the interaction between the scaffold and the cells, providing a more favorable environment for attachment and proliferation. Cell viability data showed that more than 50% of cells were viable after

days 1, 3, and 7. The highly statistically significant results (*i.e.*, $P < 0.001$) attained in the ANOVA test indicate that the cell viability rate stood astoundingly at 96% in the SA/CNF/PG/CC-3 hydrogels on day 7. Degradation analysis of the SA-containing hydrogel revealed a degradation rate of 35.9% over 28 days, indicating the hydrogel's stability. To the best of our knowledge, no prior studies have exhibited 3D-printed artificial cornea using aligned fibrous bio-ink. The inclusion of PG effectively improved the mechanical strength of the hydrogel, allowing it to be implanted in the cornea without causing an inflammatory effect. This work further illustrates that the low molarity PG can easily crosslink after 3D printing, enhancing surface morphology and mechanical properties without compromising transparency. In the future, 3D-printed cornea could potentially be used for clinical applications.

Acknowledgments

The authors are thankful to Yu-Ting Lin for helping during cell experiments.

Funding

The financial support from National Science and Technology Council (NSTC), Taiwan (Grant Nos. 111-2221-E-131-019-MY3, 111-2221-E-182-040-MY3, 111-2221-E-002-029, 112-2622-E-131-001, 112-2628-E-131-001-MY4, 113-2628-E-182-001-MY4), is highly appreciated. The author expresses gratitude for the financial support provided by Chang Gung University (URRPD2N0011 and URRPD2N0031).

Conflict of interest

The authors declare they have no conflicts of interests.

Author contributions

Conceptualization: Wei-Fang Su, Meng-Fang Lin, Yu-Ching Huang

Formal analysis: Priyanka Chaudhary, Chun-Yu Chang, Ting-Han Lin, Ming-Chung Wu

Funding Acquisition: Ming-Chung Wu, Meng-Fang Lin, Yu-Ching Huang

Investigation: Priyanka Chaudhary, Chia-Hsien Lee

Methodology: Priyanka Chaudhary, Dun-Heng Tan

Resource: Meng-Fang Lin, Yu-Ching Huang

Supervision: Wei-Fang Su, Meng-Fang Lin, Yu-Ching Huang

Writing – original draft: Priyanka Chaudhary, Meng-Fang Lin

Writing – review & editing: Wei-Fang Su, Meng-Fang Lin, Yu-Ching Huang

Ethics approval and consent to participate

Not applicable.

Consent for publication

Not applicable.

Availability of data

The data included in this study is available upon reasonable request from the corresponding author.

References

- Kong B, Chen Y, Liu R, et al. Fiber reinforced GelMA hydrogel to induce the regeneration of corneal stroma. *Nat Commun.* 2020;11(1):1435. doi: 10.1038/s41467-020-14887-9.
- Ahn J-I, Kuffova L, Merrett K, et al. Crosslinked collagen hydrogels as corneal implants: effects of sterically bulky vs. non-bulky carbodiimides as crosslinkers. *Acta biomaterialia.* 2013;9(8):7796-7805. doi: 10.1016/j.actbio.2013.04.014.
- Griffith M, Hakim M, Shimmura S, et al. Artificial human corneas: scaffolds for transplantation and host regeneration. *Cornea.* 2002;21:S54-S61. doi: 10.1097/01.icc.0000263120.68768.f8.
- Gain P, Jullienne R, He Z, et al. Global survey of corneal transplantation and eye banking. *JAMA ophthalmology.* 2016;134(2):167-173. doi: 10.1001/jamaophthalmol.2015.4776.
- Bentley E, Murphy CJ, Li F, Carlsson DJ, Griffith M. Biosynthetic corneal substitute implantation in dogs. *Cornea.* 2010;29(8):910-916. doi: 10.1097/ICO.0b013e3181c846aa.
- Liu L, Kuffová L, Griffith M, et al. Immunological responses in mice to full-thickness corneal grafts engineered from porcine collagen. *Biomaterials.* 2007;28(26):3807-3814. doi: 10.1016/j.biomaterials.2007.04.025.
- San Choi J, Williams JK, Greven M, et al. Bioengineering endothelialized neo-corneas using donor-derived corneal endothelial cells and decellularized corneal stroma. *Biomaterials.* 2010;31(26):6738-6745. doi: 10.1016/j.biomaterials.2010.05.020.
- Armitage WJ, Goodchild C, Griffin MD, et al. High-risk corneal transplantation: recent developments and future possibilities. *Transplantation.* 2019;103(12):2468-2478. doi: 10.1097/TP.0000000000002938.
- Grigoryan B, Paulsen SJ, Corbett DC, et al. Multivascular networks and functional intravascular topologies within biocompatible hydrogels. *Science.* 2019;364(6439):458-464. doi: 10.1126/science.aav9750
- Orash Mahmoud Salehi A, Heidari-Keshel S, Poursamar SA, et al. Bioprinted membranes for corneal tissue engineering: a review. *Pharmaceutics.* 2022;14(12):2797. doi: 10.3390/pharmaceutics14122797.

11. Alam F, Elsharif M, AlQattan B, et al. 3D printed contact lenses. *ACS Biomater Sci Eng.* 2021;7(2):794-803. doi: 10.1021/acsbmaterials.0c01470
12. Alam F, Alsharif A, AlModaf FO, El-Atab N. 3D-printed smartwatch fabricated via vat photopolymerization for UV and temperature sensing applications. *ACS Omega.* 2024;9(13):14830-14839. doi: 10.1021/acsomega.3c07411.
13. Bernal PN, Delrot P, Loterie D, et al. Volumetric bioprinting of complex living-tissue constructs within seconds. *Adv Mater.* 2019;31(42):1904209. doi: 10.1002/adma.201904209
14. Patel AP, Wu EI, Ritterband DC, Seedor JA. Boston type 1 keratoprosthesis: the New York Eye and Ear experience. *Eye (Lond).* 2012;26(3):418-425. doi: 10.1038/eye.2011.325
15. Zhang X, Zhang X, Li Y, Zhang Y, et al. Applications of Light-Based 3D Bioprinting and Photoactive Biomaterials for Tissue Engineering. *Materials.* 2023;16(23):7461 doi: 10.3390/ma16237461
16. Riau AK, Venkatraman SS, Dohlman CH, Mehta JS. Surface modifications of the PMMA optic of a keratoprosthesis to improve biointegration. *Cornea.* 2017;36:S15-S25. doi: 10.1097/ICO.0000000000001352
17. Ma T-L, Yang S-C, Cheng T, et al. Exploration of biomimetic poly (γ -benzyl-L-glutamate) fibrous scaffolds for corneal nerve regeneration. *J Mater Chem B.* 2022;10(33):6372-6379. doi: 10.1038/s41536-017-0038-8
18. Islam MM, Buznyk O, Reddy JC, et al. Biomaterials-enabled cornea regeneration in patients at high risk for rejection of donor tissue transplantation. *NPJ Regen Med.* 2018;3(1):2. doi: 10.1038/s41536-017-0038-8
19. Mimura T, Amano S, Yokoo S, et al. Tissue engineering of corneal stroma with rabbit fibroblast precursors and gelatin hydrogels. *Mol Vis.* 2008;14:1819.
20. Crabb RA, Chau EP, Evans MC, Barocas VH, Hubel A. Biomechanical and microstructural characteristics of a collagen film-based corneal stroma equivalent. *Tissue Eng.* 2006;12(6):1565-1575. doi: 10.1089/ten.2006.12.1565
21. Lawrence BD, Marchant JK, Pindrus MA, Omenetto FG, Kaplan DL. Silk film biomaterials for cornea tissue engineering. *Biomaterials.* 2009;30(7):1299-1308. doi: 10.1016/j.biomaterials.2008.11.018
22. Gouveia RM, González-Andrades E, Cardona JC, et al. Controlling the 3D architecture of Self-Lifting Auto-generated Tissue Equivalents (SLATEs) for optimized corneal graft composition and stability. *Biomaterials.* 2017;121:205-219. doi: 10.1016/j.biomaterials.2016.12.023.
23. Wang S, Ghezzi CE, Gomes R, Pollard RE, Funderburgh JL, Kaplan DL. In vitro 3D corneal tissue model with epithelium, stroma, and innervation. *Biomaterials.* 2017;112:1-9. doi: 10.1016/j.biomaterials.2016.09.030
24. Dong H, Snyder JF, Williams KS, Andzelm JW. Cation-induced hydrogels of cellulose nanofibrils with tunable moduli. *Biomacromolecules.* 2013;14(9):3338-3345. doi: 10.1021/bm400993f
25. Yang J, Han C-R, Duan J-F, et al. Studies on the properties and formation mechanism of flexible nanocomposite hydrogels from cellulose nanocrystals and poly (acrylic acid). *J Mater Chem.* 2012;22(42):22467-22480. doi: 10.1039/C2JM35498E
26. Yu TY, Tseng YH, Wang CC, et al. Three-level hierarchical 3D network formation and structure elucidation of wet hydrogel of tunable-high-strength nanocomposites. *Macromol Mater Eng.* 2022;307(5):2100871. doi: 10.1002/mame.202100871
27. Rafat M, Li F, Fagerholm P, et al. PEG-stabilized carbodiimide crosslinked collagen-chitosan hydrogels for corneal tissue engineering. *Biomaterials.* 2008;29(29):3960-3972. doi: 10.1016/j.biomaterials.2008.06.017
28. Wang J, Gao C, Zhang Y, Wan Y. Preparation and in vitro characterization of BC/PVA hydrogel composite for its potential use as artificial cornea biomaterial. *Mater Sci Eng C.* 2010;30(1):214-218. doi: 10.1016/j.msec.2009.10.006
29. Brunette I, Roberts CJ, Vidal F, et al. Alternatives to eye bank native tissue for corneal stromal replacement. *Prog Retin Eye Res.* 2017;59:97-130. doi: 10.1016/j.preteyeres.2017.04.002
30. Nie X, Tang Y, Wu T, et al. 3D printing sequentially strengthening high-strength natural polymer hydrogel bilayer scaffold for cornea regeneration. *Regen Biomater.* 2024;11:rbae012.
31. Romo-Valera C, Guerrero P, Arluzea J, Etxebarria J, de la Caba K, Andollo N. Cytocompatibility and suitability of protein-based biomaterials as potential candidates for corneal tissue engineering. *Int J Mol Sci.* 2021;22(7):3648.
32. Liu J, Huang Y, Yang W, et al. Sutureless transplantation using a semi-interpenetrating polymer network bioadhesive for ocular surface reconstruction. *Acta Biomater.* 2022;153:273-286. doi: 10.1016/j.actbio.2022.09.049
33. Rastogi P, Kandasubramanian B. Review of alginate-based hydrogel bioprinting for application in tissue engineering. *Biofabrication.* 2019;11(4):042001. doi: 10.1088/1758-5090/ab331e
34. Logan CM, Fernandes-Cunha GM, Chen F, et al. In situ-forming collagen hydrogels crosslinked by multifunctional polyethylene glycol as a matrix therapy for corneal defects: 2-month follow-up in vivo. *Cornea.* 2023;42(1):97-104.

- doi: 10.1097/ICO.0000000000003104
35. Raus RA, Nawawi WMFW, Nasaruddin RR. Alginate and alginate composites for biomedical applications. *Asian J Pharm Sci.* 2021;16(3):280-306. doi: 10.1016/j.ajps.2020.10.001
 36. Zarrintaj P, Ghorbani S, Barani M, et al. Polylysine for skin regeneration: a review of recent advances and future perspectives. *Bioeng Transl Med.* 2022;7(1):e10261. doi: 10.1002/btm2.10261
 37. Wang L, Zhang HJ, Liu X, et al. A physically cross-linked sodium alginate–gelatin hydrogel with high mechanical strength. *ACS Appl Polym Mater.* 2021;3(6):3197-3205. doi: 10.1021/acscapm.1c00404
 38. Reddy MSB, Ponnamma D, Choudhary R, Sadasivuni KK. A comparative review of natural and synthetic biopolymer composite scaffolds. *Polymers.* 2021;13(7):1105. doi: 10.3390/polym13071105
 39. Yue X, Deng W, Zhou Z, Xu Y, He J, Wang Z. Reinforced and flame retarded cellulose nanofibril/sodium alginate compound aerogel fabricated via boric acid/Ca²⁺ double cross-linking. *J Polym Environ.* 2023;31(3):1038-1050.
 40. Zander ZK, Hua G, Wiener CG, Vogt BD, Becker ML. Control of mesh size and modulus by kinetically dependent cross-linking in hydrogels. *Adv Mater.* 2015;27(40):6283. doi: 10.1002/adma.201501822
 41. Kim S-S, Park MS, Jeon O, Choi CY, Kim B-S. Poly (lactide-co-glycolide)/hydroxyapatite composite scaffolds for bone tissue engineering. *Biomaterials.* 2006;27(8):1399-1409. doi: 10.1016/j.biomaterials.2005.08.016
 42. Donnalaja F, Jacchetti E, Soncini M, Raimondi MT. Natural and synthetic polymers for bone scaffolds optimization. *Polymers.* 2020;12(4):905. doi: 10.3390/polym12040905
 43. Cui Y, Liu Y, Cui Y, Jing X, Zhang P, Chen X. The nanocomposite scaffold of poly (lactide-co-glycolide) and hydroxyapatite surface-grafted with L-lactic acid oligomer for bone repair. *Acta Biomater.* 2009;5(7):2680-2692. doi: 10.1016/j.actbio.2009.03.024
 44. Wang S, Li T, Chen C, et al. Transparent, anisotropic biofilm with aligned bacterial cellulose nanofibers. *Adv Funct Mater.* 2018;28(24):1707491. doi: 10.1002/adfm.201707491
 45. Wang X, Majumdar S, Soiberman U, et al. Multifunctional synthetic Bowman's membrane-stromal biomimetic for corneal reconstruction. *Biomaterials.* 2020;241:119880. doi: 10.1016/j.biomaterials.2020.119880
 46. Kong B, Sun W, Chen G, et al. Tissue-engineered cornea constructed with compressed collagen and laser-perforated electrospun mat. *Sci Rep.* 2017;7(1):970. doi: 10.1038/s41598-017-01072-0.
 47. Majumdar S, Wang X, Sommerfeld SD, et al. Cyclodextrin modulated type I collagen self-assembly to engineer biomimetic cornea implants. *Adv Funct Mater.* 2018;28(41):1804076. doi: 10.1002/adfm.201804076
 48. Lei X, Jia Y-G, Song W, et al. Mechanical and optical properties of reinforced collagen membranes for corneal regeneration through polyrotaxane cross-linking. *ACS Appl Bio Mater.* 2019;2(9):3861-3869. doi: 10.1021/acscabm.9b00464
 49. Zhang J, Sisley AM, Anderson AJ, Taberner AJ, McGhee CN, Patel DV. Characterization of a novel collagen scaffold for corneal tissue engineering. *Tissue Eng Part C Methods.* 2016;22(2):165-172. doi: 10.1089/ten.TEC.2015.0304
 50. Long Y, Zhao X, Liu S, et al. Collagen–hydroxypropyl methylcellulose membranes for corneal regeneration. *ACS Omega.* 2018;3(1):1269-1275. doi: 10.1021/acsomega.7b01511
 51. Fernandes-Cunha GM, Chen KM, Chen F, et al. In situ-forming collagen hydrogel crosslinked via multi-functional PEG as a matrix therapy for corneal defects. *Sci Rep.* 2020;10(1):16671. doi: 10.1038/s41598-020-72978-5
 52. Lei M, Zhang S, Zhou H, et al. Electrical signal initiates kinetic assembly of collagen to construct optically transparent and geometry customized artificial cornea substitutes. *ACS Nano.* 2022;16(7):10632-10646. doi: 10.1021/acsnano.2c02291
 53. Mallet JD, Rochette PJ. Wavelength-dependent ultraviolet induction of cyclobutane pyrimidine dimers in the human cornea. *Photochem Photobiol Sci.* 2013;12(8):1310-1318. doi: 10.1039/c3pp25408a.
 54. Paul A, Eun C-J, Song JM. Cytotoxicity mechanism of non-viral carriers polyethylenimine and poly-L-lysine using real time high-content cellular assay. *Polymer.* 2014;55(20):5178-5188. doi: 10.1016/j.polymer.2014.08.043
 55. Arnold Jr L, Dagan A, Gutheil J, Kaplan N. Antineoplastic activity of poly (L-lysine) with some ascites tumor cells. *Proc Natl Acad Sci.* 1979;76(7):3246-3250.
 56. Liu S, Huang D, Hu Y, et al. Sodium alginate/collagen composite multiscale porous scaffolds containing poly (ϵ -caprolactone) microspheres fabricated based on additive manufacturing technology. *RSC Adv.* 2020;10(64):39241-39250. doi: 10.1039/d0ra04581k
 57. Formisano N, van der Putten C, Grant R, et al. Mechanical properties of bioengineered corneal stroma. *Adv Health Mater.* 2021;10(20):2100972. doi: 10.1002/adhm.202100972.